Original Research

Scott A. Bradford*
Saeed Torkzaban
Andreas Wiegmann

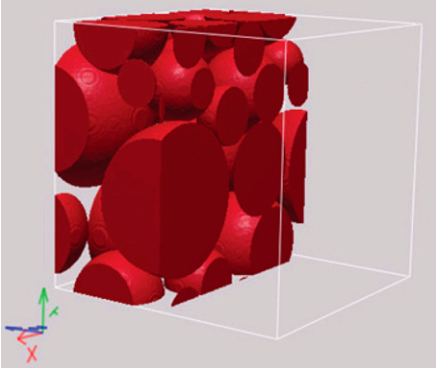

Counteracting hydrodynamic and adhesive torques determine whether a colloid will immobilize or roll on a solid. We use pore-scale simulations and scaling methods to predict the cumulative density function of hydrodynamic torque in sphere packs, and quantify the fraction of and locations on the solid surfaces that contribute to colloid retention.

S.A. Bradford, USDA-ARS, U.S. Salinity Lab., 450 W. Big Springs Rd., Riverside, CA 92507; S. Torkzaban, Earth Sciences Division, Lawrence Berkeley National Lab., Berkeley, CA; A. Wiegmann, Fraunhofer ITWM, Kaiserslautern, Germany. *Corresponding author (Scott.Bradford@ars.usda.gov).

Vadose Zone J. 10:252–261
doi:10.2136/vzj2010.0064
Received 5 May 2010.
Published online 14 Dec. 2010.

Pore-Scale Simulations to Determine the Applied Hydrodynamic Torque and Colloid Immobilization

Values of the applied hydrodynamic torque ($T_{applied}$) and the resisting adhesive torque ($T_{adhesion}$) will determine whether a colloid will be immobilized ($T_{applied} \leq T_{adhesion}$) or roll ($T_{applied} > T_{adhesion}$) on a solid water interface. Previous literature has demonstrated in 1–2 collector (grain) systems that the influence of $T_{applied}$ on colloid retention can be significant under unfavorable attachment conditions and that only a fraction of the solid surface may contribute to retention. However, many questions remain on how to obtain, analyze, and upscale information on the forces and torques that act on colloids near solid surfaces in porous media. To address some of these gaps in knowledge, high resolution pore-scale water flow simulations were conducted for sphere packs (25 spheres) over a range of Darcy velocities, grain sizes and distributions, and porosities. The spatial variability of $T_{applied}$ was calculated from this information, and successfully described using a lognormal cumulative density function (CDF). Linear interpolation and scaling techniques were subsequently used to predict the lognormal CDF of $T_{applied}$ for various colloid sizes, grain sizes and distributions, and water velocities. The lognormal CDF of $T_{applied}$ was then evaluated at select values of $T_{adhesion}$ (i.e, interaction energy) to quantify the fraction and locations on the solid surface that contributes to colloid retention (S_f), and the theoretical maximum solid phase concentration of retained colloids (S_{max}).

Abbreviations: CDF, cumulative density function; DLVO, Derjaguin–Landau–Verwey–Overbeek [theory]; IS, ionic strength; JKR, Johnson, Kendall, and Roberts [theory]; SWI, solid–water interface.

Recent research has demonstrated that colloid retention does not depend solely on the strength of the adhesive interaction (Bradford et al., 2007, 2009; Johnson et al., 2007a; Torkzaban et al., 2007, 2008; Bradford and Torkzaban, 2008; Duffadar and Davis, 2008; Shen et al., 2008). Findings suggest that colloid retention in porous media depends on the chemistry of the aqueous and solid phases, as well as the pore structure and surface roughness, the colloid size and concentration, and water velocity. In particular, colloids that are weakly associated with the solid–water interface (SWI) via the secondary minimum or nanoscale heterogeneity may roll, slide, skip, or detach on/from the collector surface because of hydrodynamic forces during fluid flow (Torkzaban et al., 2007, 2008; Bradford and Torkzaban, 2008; Duffadar and Davis, 2008). Fluid drag force can translate and/or funnel these colloids on the SWI to locations where they can be retained (Torkzaban et al., 2007, 2008; Bradford and Torkzaban, 2008; Kuznar and Elimelech, 2007), for example, in regions associated with lower velocities (grain–grain contacts and surface roughness) or increased adhesion (chemical heterogeneity).

Torkzaban et al. (2007, 2008) theoretically studied the influence of hydrodynamic and adhesive forces and torques on colloid attachment to one or two spheroidal (spheres and ellipsoids) collectors. These authors found that under unfavorable attachment conditions only a fraction of the collector surface area (S_f) contributed to colloid attachment during water flow due to spatial variability in the hydraulic forces and torques near the collector surfaces. The size, shape, and number of collectors; the colloid size; and the average water velocity influenced these hydrodynamic forces, and therefore S_f. Similarly, factors that influenced the adhesive forces and torques (e.g, colloid size, ionic strength, and the charge of the colloid and collectors) were also demonstrated to influence S_f. These results have important implications for determining the fractions of the solid surface that contributes to colloid deposition and release; that is, colloids are immobilized in the region defined by S_f, whereas colloids are mobile (roll) in the region defined by $(1 - S_f)$. As S_f fills with retained colloids, the retention rate will decrease with time and/or concentration. Indeed, the value of S_f has previously been related to the maximum solid phase colloid

concentration (Bradford et al., 2009; Kim et al., 2009), S_{max}, in the Langmuirian blocking function (Adamczyk et al., 1994).

The above studies provided useful information to understand the influence of hydrodynamics and adhesive forces on colloid retention under unfavorable attachment conditions. Nevertheless, significant gaps in knowledge still remain that inhibit the use of pore-scale hydrodynamic forces and torques to study colloid retention at larger spatial scales. For example, computational limitations currently exist for the grid size and resolution that the governing pore-scale flow equations can be solved on. Other difficulties arise in accurately describing realistic pore space geometries that account for different grain sizes and distributions, grain–grain contacts, porosities, and pore-water velocities. Questions also remain about how to upscale pore-scale information on the hydrodynamic and adhesive forces and torques. This is especially true when the hydrodynamic forces are spatially variable due to differences in pore geometry. In this work we attempt to theoretically address these gaps in knowledge through the use of state-of-the-art modeling of pore-scale fluid flow in various sphere packs, scaling techniques, calculated probability density functions for the applied hydrodynamic torque, and torque balance.

Theory

Forces and Torques

A colloid that collides with an interface may attach, translate over the surface, or detach in the presence of water flow. Lifting, sliding, and rolling are the hydrodynamic mechanisms that can cause colloid removal from an interface (Soltani and Ahmadi, 1994; Bergendahl and Grasso, 1998, 2000). We will briefly consider the forces and torques that act on the colloids near the SWI to determine the appropriate criteria for colloid immobilization and removal. This analysis assumes that the roughness on the colloid surface and SWI is small relative to the colloid size. Modified theory is needed to describe similar forces and torques when the roughness is of a similar size as the colloid (Vaidyanathan and Tien, 1988).

Hydrodynamic forces will act on colloids that are in the vicinity of the SWI when water flows through porous media. The lift force (F_L, M L T^{-2}) acting on the colloid perpendicular to the SWI is negligible when the flow is laminar (Soltani and Ahmadi, 1994). Conversely, the drag force (F_D, M L T^{-2}) that acts on the colloid tangential to the interface at a separation distance (h, L) is significant and is given as (Goldman et al., 1967; O'Neill, 1968; Duffadar and Davis, 2008):

$$F_D = 6\pi\mu_w\tau_w r_c\left(r_c + h\right)C_h \quad [1]$$

where r_c [L] is the colloid radius, τ_w [T^{-1}] is the hydrodynamic shear, μ_w [M L^{-1} T^{-1}] is the water viscosity, and C_h is a dimensionless function that depends on h as (Duffadar and Davis, 2008):

$$C_h = \frac{1.7007337 + 1.0221616\left(h/r_c\right)}{1 + 1.0458291\left(h/r_c\right) - 0.0014884708\left(h/r_c\right)^2} \quad [2]$$

On a smooth surface the value of the applied hydrodynamic torque ($T_{applied}$, M L^2 T^{-2}) that acts on the colloid at h is given as (Duffadar and Davis, 2008):

$$T_{applied} = r_c F_D + 4\pi\mu_w\tau_w r_c^3 C_{2h} \quad [3]$$

In this case, C_{2h} is a second dimensionless function that depends on h as (Duffadar and Davis, 2008):

$$C_{2h} = 0.054651334\left\{18.276952 - \exp\left[-1.422943\left(h/r_c\right)\right]\right\} \quad [4]$$

When r_c is much greater than h, the value of $T_{applied}$ is more simply given as (Goldman et al., 1967; O'Neill, 1968; Torkzaban et al., 2007):

$$T_{applied} = 14.287\pi\mu_w\tau_w r_c^3 \quad [5]$$

Derjaguin–Landau–Verwey–Overbeek (DLVO) theory (Derjaguin and Landau, 1941; Verwey and Overbeek, 1948) is commonly used to estimate the interaction energy of colloids with spherical collectors (grains). A sphere–plate interaction is assumed when the size of the colloid is small relative to the collector, otherwise a sphere–sphere interaction is employed (Elimelech et al., 1995). The net adhesive force (F_A, M L T^{-2}) that is required to mobilize a colloid from a minimum in the interaction energy can be calculated using the Derjaguin and Langbein approximations as (Israelachvili, 1992):

$$F_A = \frac{2\pi r_c\Phi_{min}}{A_{eff}} = \frac{2\pi r_c\Phi_{min}}{2\pi r_c h} = \frac{\Phi_{min}}{h} \quad [6]$$

where Φ_{min} [M L^2 T^{-2}] is the absolute value of the minimum in the interaction energy, and A_{eff} [L^2] is the effective interaction area between a sphere and a flat surface. This equation holds when $h << r_c$.

Adhesive interaction of a colloid with the SWI occurs at a small separation distance, and only a portion of the colloid's projection on the SWI makes a meaningful contribution to F_A (Israelachvili, 1992). This zone of adhesive influence (Duffadar and Davis, 2007) will produce an adhesive or resisting torque ($T_{adhesion}$; M L^2 T^{-2}) and a corresponding frictional force (F_F, M L T^{-2}) that acts tangential to the SWI in the direction opposite to F_D (e.g., Bergendahl and Grasso, 1998; Duffadar and Davis, 2008). The values of $T_{adhesion}$ and F_F are defined as (Bergendahl and Grasso, 1998; Lindeburg, 2001):

$$T_{adhesion} = l_x F_A \quad [7]$$

$$F_F = \mu_f F_A \quad [8]$$

where l_x [L] is the lever arm and μ_f is the coefficient of friction. The values of l_x and μ_f are related to each other through (Lindeburg, 2001):

$$l_x = \mu_f r_c \quad [9]$$

This mathematical description (Eq. [7–9]) is valid for resistance due to both deformation and friction (Lindeburg, 2001). However, relatively few methods currently exist to estimate l_x in the zone of adhesive influence. Theory by Johnson, Kendall, and Roberts (JKR) has been developed to account for resistance due to deformation (Johnson et al., 1971), and this theory has been used to quantify l_x under favorable (Bergendahl and Grasso, 2000) and unfavorable (Bradford et al., 2007; Torkzaban et al., 2007) attachment conditions. For primary minimum interaction on a smooth surface the value of l_x is given as:

$$l_x = \left(\frac{4F_A r_c}{K}\right)^{1/3} \quad [10]$$

Here K [M L^{-1} T^{-2}] is the composite Young's modulus ($K = 4.014 \times 10^9$ N m^{-2} for glass bead collectors and a polystyrene colloid suspension). For interaction at a separation distance due to the secondary minimum or nanoscale chemical heterogeneity the value of l_x is given as (Johnson et al., 1971):

$$l_x = \left(\frac{F_A r_c}{K}\right)^{1/3} \quad [11]$$

Alternatively, others have attributed l_x to friction that arises from surface roughness, and assumed an empirical value of $\mu_f = 1.3 \times 10^{-4}$ in simulations of colloid trajectories over a SWI having positively charged nanoscale heterogeneity (Duffadar and Davis, 2008).

For the purposes of this work, the exact cause/form of l_x is not the most critical question, but rather that l_x must occur to have colloid immobilization in the presence of water flow. If $l_x = 0$, then no colloid immobilization will occur on the SWI under favorable or unfavorable conditions, because F_A and F_D are perpendicular. This prediction is not consistent with many experimental observations that support the existence of l_x, which are summarized in Torkzaban et al. (2009, 2010), including microscopic observations of colloid immobilization, significant amounts of colloid retention, and colloid release with changes in the solution chemistry.

It should be mentioned that in some researchers have neglected l_x when colloids interact with the solid surface at a separation distance (e.g., via the secondary minimum or nanoscale heterogeneity), but have implicitly accounted for l_x by assuming that colloid immobilization occurs in the primary minimum when the separation distance is zero (Yang et al., 1998; Johnson et al., 2007b). However, one should note that in aquatic environments the separation distance is not zero even for interaction in the primary minimum due to the presence of Born repulsion and repulsive hydration forces (Elimelech et al., 1995).

Force and torque balances can be used to determine criteria for colloid removal via rolling and sliding, and colloid immobilization (Bergendahl and Grasso, 1998). Colloids will roll over the SWI when $T_{applied} > T_{adhesion}$. This inequality may be rewritten in terms of a critical value of hydrodynamic shear to initiate rolling (τ_{cr}, T^{-1}) using Eq. [1], [3], and [7] as:

$$\tau_{cr} > \frac{l_x F_A}{\pi\mu_w\left[6r_c^2(r_c+h)C_h + 4r_c^3 C_{2h}\right]} \quad [12]$$

Conversely, colloids will slide over the SWI when $F_D > F_F$. Similarly to Eq. [12], we can determine a critical value of hydrodynamic shear to initiate sliding (τ_{cs}, T^{-1}) using Eq. [1], [8], and [9] to rewrite this inequality as:

$$\tau_{cs} > \frac{l_x F_A}{\pi\mu_w\left[6r_c^2(r_c+h)C_h\right]} \quad [13]$$

The only difference in Eq. [12] and [13] is the extra term in the denominator on the right-hand side of Eq. [12], and this indicates that τ_{cr} will be less than τ_{cs}. Consequently, rolling will be the dominant hydrodynamic mechanism of colloid removal from the SWI under laminar flow conditions, as has previously been reported (Tsai et al., 1991; Bergendahl and Grasso, 1998, 1999), and colloid immobilization occurs when $T_{applied} \leq T_{adhesion}$. These findings hold when colloids interact with the SWI at a separation distance (primary and secondary minima, and nanoscale heterogeneity) and are independent of the selected description of the level arm (using Eq. [10], [11], or an empirical value).

The torque balance approach described above has previously been used to determine S_f for one or two smooth collectors (Torkzaban et al., 2007, 2008). A knowledge of the distribution of $T_{applied}$ and $T_{adhesion}$, which vary with the pore space geometry and chemical heterogeneity (colloid and SWI), is required to apply this approach to conditions that are more representative of natural porous media. The emphasis in this work is on quantifying $T_{applied}$ in relatively simple sphere packs that encompass collector diameters (d_{50}, L) ranging from 50 to 5000 μm, with coefficients of uniformity (U_i) from 1 to 6, porosities (ε) of 0.28 to 0.36, and Darcy water velocities (q, L T^{-1}) from 2.1×10^{-6} to 2.1×10^{-3} m s^{-1}. Uniform values of $T_{adhesion}$ were assumed to determine S_f under idealized conditions (no chemical heterogeneity). However, it should be mentioned the torque balance approach may also be applied to determine S_f under chemically heterogeneous conditions (Bradford and Torkzaban, 2008).

Computer Simulations of Pore-Scale Water Flow

The GEODICT commercial software package (Fraunhofer Institut fur Techno- und Wirtschaftsmathematik ITWM, 2003) was used

to generate sphere packs of various collector sizes and distributions and to solve the three-dimensional governing equations for pore-scale water flow. The sphere packs were generated using an algorithm based on the Forced Biased Algorithm (Bezrukov et al., 2001; Torquato, 2002) that includes grain–grain contacts. Pore-scale water flow in the sphere packs was described using the Stokes and continuity equations under steady-state laminar flow conditions:

$$\nabla p = \mu_w \nabla^2 \mathbf{v} + \rho \mathbf{g} \quad [14]$$

$$\nabla \cdot \mathbf{v} = 0 \quad [15]$$

where ρ [M L^{-3}] is the fluid density, $\mathbf{v}$ [L T^{-1}] is the velocity vector, p [M L^{-1} T^{-2}] is pressure, and $\mathbf{g}$ [L T^{-2}] is the acceleration due to gravity vector. GEODICT solves these equations using a modified version of the explicit jump finite difference approach (Wiegmann and Bube, 2000; Wiegmann, 2007) that overcomes previously reported limitations with regard to simulation porosities. The normal velocity and tangential stress at the side boundaries of the simulation domain were set equal to zero. A constant flux was imposed between the inlet and outlet of the simulation domain to achieve steady-state flow at a selected velocity. A no-slip boundary condition was imposed along the collector surfaces. The solution of these water flow equations has been extensively verified by comparison with results from other software packages and numerical techniques (Fraunhofer Institut fur Techno- und Wirtschaftsmathematik ITWM, 2003; Tafreshi et al., 2009).

The simulation domain was discretized into 256 × 256 × 256 equally sized voxels (a total of 1.67 × 10^7). This resolution was selected based on consideration of the computational limitations of our computer system, a Hewlett-Packard Z800 with two quad core Intel Xeon X5550 processors, 48 GB of RAM, and a 64 bit Windows XP operating system. All simulations were performed on sphere packs that were made up of 25 collectors. These conditions allowed us to achieve a high resolution flow field, with the voxel length approximately equal to 1% of the median collector diameter.

Following completion of the pore-scale water flow simulations, the water flow velocities of the voxels along the collector boundaries were extracted and used to determine τ_w and $T_{applied}$. The use of this boundary velocity information was further extended to a wider range of conditions by linear interpolation and scaling techniques. For simplicity we have employed Eq. [5] to determine $T_{applied}$ because it is independent of h (i.e., assumes that $r_c >> h$). Alternatively, Eq. [3] could also have been used, but then $T_{applied}$ and F_A are both functions of h. The CDF of $T_{applied}$ was subsequently determined from this information and used to determine S_f for a given value of $T_{adhesion}$. This analysis assumes that the simulated flow field was independent of colloids in solution or attached to the SWI and is strictly valid only for dilute colloidal suspensions and clean bed conditions.

Results and Discussion

Analysis of One Sphere Pack

An illustrative example of the pore structure, simulated flow field, and the CDF for $T_{applied}$ in the sphere packs is given in Fig. 1a, 1b, and 1c, respectively. The simulation conditions were for r_c = 0.5 μm, d_{50} = 500 μm, U_i = 2.08 (9 sphere classes ranging from 250 to 750 μm having equal mass fractions), ε = 0.3, and q = 8.4 × 10^{-6} m s^{-1}. The minimum, median, and maximum values of $T_{applied}$ were 1.25 × 10^{-21}, 1.61 × 10^{-20}, and 2.45 × 10^{-19} N m, respectively. Hence, the value of $T_{applied}$ ranged over more than two orders of magnitude. The implications of such variations in $T_{applied}$ on colloid retention will be discussed later.

Linear interpolation and scaling techniques were employed to extend the simulated flow fields to a wide range of conditions. Boundary conditions dictate that the velocity is zero at the SWI, and the simulation results yield the reference boundary velocity (V_{BC1}) at a distance of one-half the voxel length ($L_{V1}/2$). Linear interpolation is then used to determine the velocity (V_1) as a function of radial distance (r) from the SWI as:

$$V_1 = \frac{2r}{L_{V1}} V_{BC1} \quad [16]$$

This assumption is justifiable under laminar flow conditions when the gradient in velocity is uniform (e.g., in a capillary tube this occurs when the tube radius is greater than r). Under steady-state flow conditions, the simulated flow field and geometry can be made dimensionless (Snyder and Stewart, 1966) and related to other conditions at a particular voxel location as:

$$\frac{V_{BC1} d_1}{q_1 L_{V1}} = \frac{V_{BC2} d_2}{q_2 L_{V2}} \quad [17]$$

where d_1 and q_1 indicate the median grain diameter and the Darcy velocity for reference condition 1, and the values of similar variables are denoted with a subscript 2 for condition 2. In Eq. [17] the flow field under condition 1 is made dimensionless by dividing by q_1, whereas the characteristic domain geometry length (e.g., L_{V1}) is made dimensionless by dividing by d_1.

Equations [16–17] can be combined and used to determine the velocity at a distance of r from the SWI under condition 2 as:

$$V_2 = \frac{2r}{L_{V1}} \left(\frac{d_1}{d_2}\right)\left(\frac{q_2}{q_1}\right) V_{BC1} \quad [18]$$

The corresponding shear rate (τ_2) and applied torque ($T_{applied2}$) are given as:

$$\tau_2 = \frac{2}{L_{V1}} \left(\frac{d_1}{d_2}\right)\left(\frac{q_2}{q_1}\right) V_{BC1} = \tau_1 \left(\frac{d_1}{d_2}\right)\left(\frac{q_2}{q_1}\right) \quad [19]$$

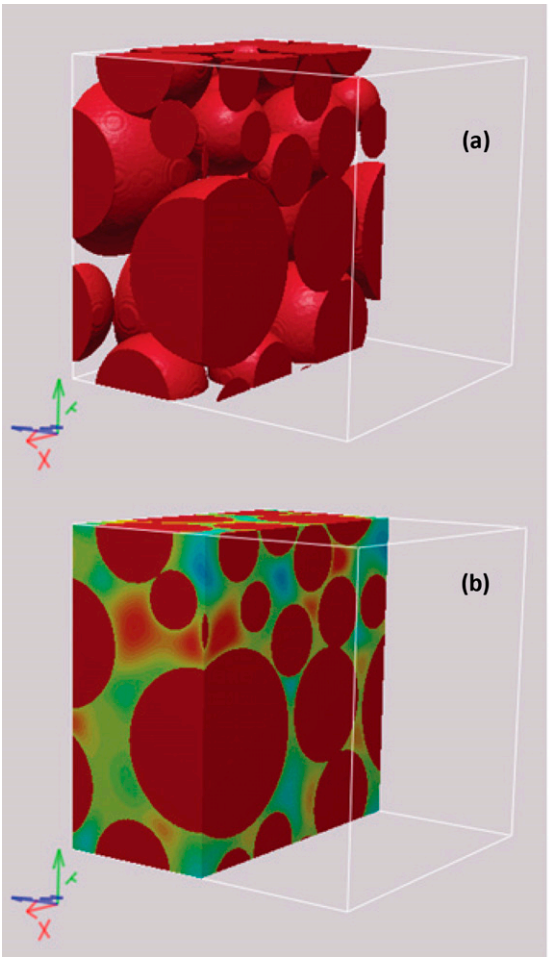

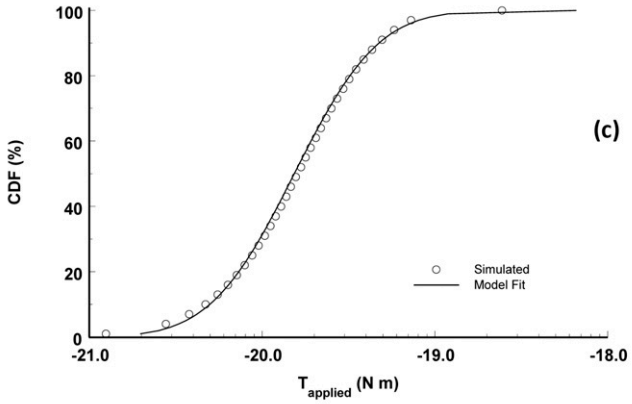

Fig. 1. An illustrative example of (a) the pore structure, (b) simulated flow field, and (c) the cumulative density function (CDF) for the applied hydrodynamic torque ($T_{applied}$) in a sphere pack. The simulation conditions were for $r_c = 0.5$ μm, $d_{50} = 500$ μm, $U_i = 2.08$, $\varepsilon = 0.3$, and $q = 8.4 \times 10^{-6}$ m s^{-1}. Also shown in (c) is the fitted lognormal CDF (Eq. [21]). The x axis of (c) is plotted on a log scale, and the numbers shown are the power of the base 10 exponent.

$$T_{applied2} = T_{applied1}\left(\frac{d_1}{d_2}\right)\left(\frac{q_2}{q_1}\right) \quad [20]$$

Equation [20] can be used to predict the CDF of $T_{applied}$ for different values of d_{50} and q, whereas the predicted influence of r_c follows directly from Eq. [5] or [3]. Representative predictions are shown in Fig. 2a, 2b, and 2c for the geometry and the reference CDF of $T_{applied}$ shown in Fig. 1. The values of r_c shown in Fig. 2a were selected to encompass the size range of various virus, bacteria, and protozoan pathogens. Note in Fig. 2 that $T_{applied}$ varies over many orders of magnitude (>10 in Fig. 2a) depending on the values of r_c, d_{50}, and q. The validity of Eq. [20] is demonstrated in Fig. 2b and 2c by comparing simulated and predicted values of the CDF for $T_{applied}$ for several different values of d_{50} and q. Further evidence for the validity of Eq. [17] at locations away from the SWI is given in Fig. 3. This figure presents a cross-section of the simulated flow field for the same geometry and velocity shown in Fig. 1 but when $d_{50} = 50$ and 5000 μm. The flow fields are nearly identical for the different values of d_{50} when the plots are scaled.

The CDF of $T_{applied}$ was characterized by fitting the parameters (mean and variance) of the lognormal CDF to the simulated data shown Fig. 1c. The lognormal CDF has the following form:

$$\mathrm{CDF}\left(T_{applied}\right) = \frac{1}{2} + \frac{1}{2}\mathrm{erf}\left[\frac{\ln(T_{applied}) - \mu}{\sigma\sqrt{2}}\right] \quad [21]$$

where μ and σ are the mean and variance of the lognormal distribution, respectively. The model fit is shown in Fig. 1c. The coefficient of regression (R^2) was 0.982, indicating that the CDF of $T_{applied}$ was well described by a lognormal distribution. It is interesting to note that field-scale velocity distributions have frequently been reported to be lognormally distributed due to a heterogeneous distribution of permeability (Toride et al., 1995). Our pore-scale simulations suggest that this same distribution can hold for homogeneous media simply due to the effects of grain geometry and distribution.

Equation [21] provides a simple framework to predict the average CDF of $T_{applied}$ for different experimental conditions. The value of μ for the lognormal distribution is defined as (Toride et al., 1995):

$$\mu = \ln\left(\left\langle T_{applied2}\right\rangle\right) - 0.5\sigma^2 \quad [22]$$

In this case, $\langle T_{applied2}\rangle$ corresponds to the average value of $T_{applied2}$ on the SWI, and it follows directly from Eq. [19] and [20]:

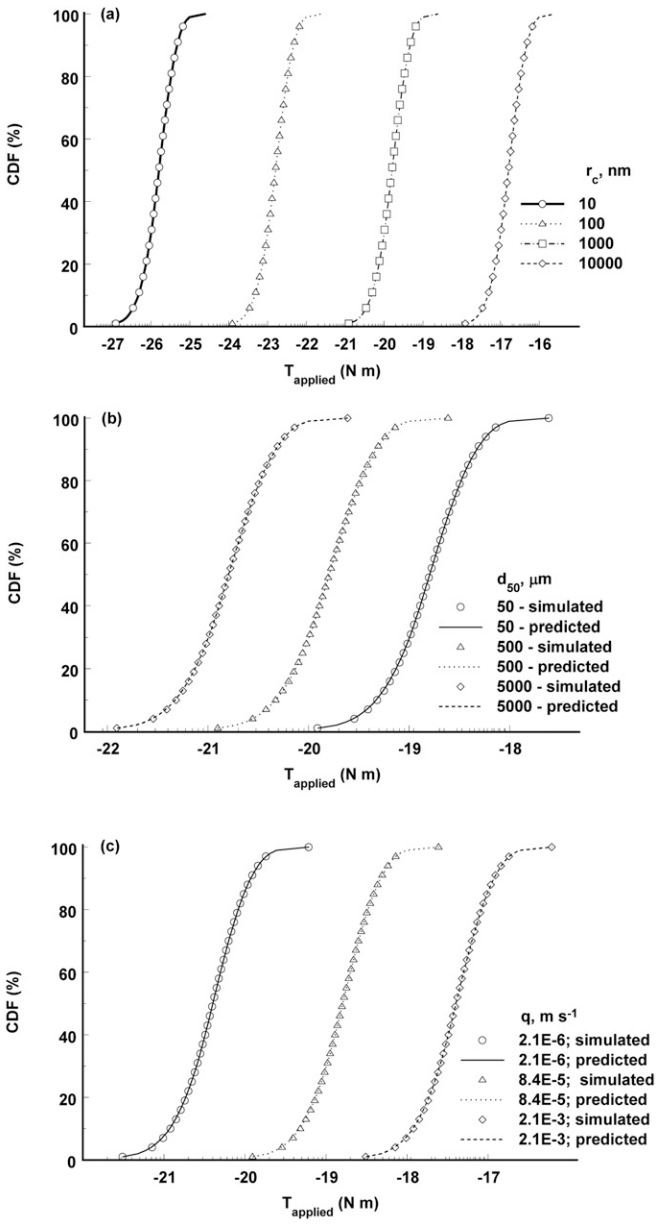

Fig. 2. The cumulative density function (CDF) for the applied hydrodynamic torque ($T_{applied}$) for various values of (a) r_c, (b) d_{50}, and (c) q indicated in the figure legends for the sphere pack geometry shown in Fig. 1. Predictions were obtained using Eq. [20] and information shown in Fig. 1c. The x axes of the figures are plotted on a log scale, and the numbers shown are the power of the base 10 exponent.

$$\left\langle T_{\text{applied2}} \right\rangle = \left\langle T_{\text{applied1}} \right\rangle \left(\frac{d_1}{d_2} \right) \left(\frac{q_2}{q_1} \right) \qquad [23]$$

For data shown in Fig. 1 the value of $<T_{applied1}> = 2.39 \times 10^{-20}$ N m and $\sigma = 0.88$. Predicted values of $T_{applied}$ for different porous media and experimental conditions may be used for comparison of colloid retention behavior in impinging jet and parallel flow chamber experiments under similar hydrodynamic conditions.

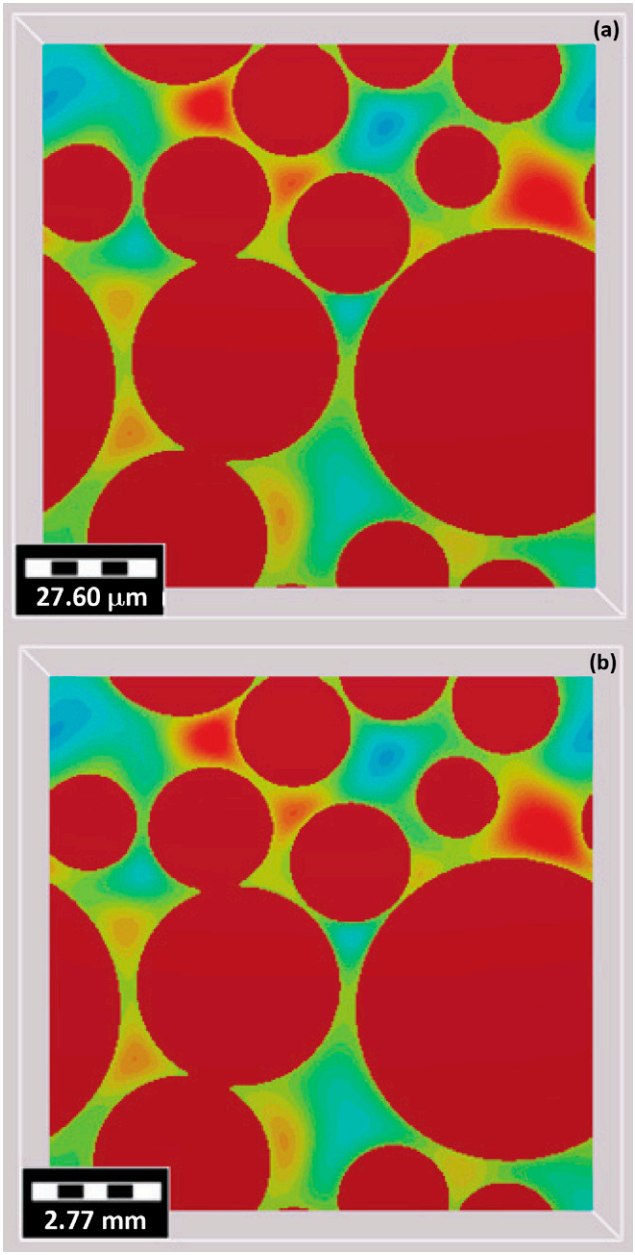

Fig. 3. Simulated flow field for the same pore geometry and velocity shown in Fig. 1a but when (a) $d_{50} = 50$ μm and (b) $d_{50} = 5000$ μm.

It should be mentioned that other CDFs (e.g., normal or Weibull distributions) may be required to describe simulated $T_{applied}$ for more complex grain size distributions. In this case, our analyses can easily be extended by simply replacing the lognormal CDF in Eq. [21–23] with similar expressions for the selected CDF.

Analysis of Multiple Sphere Packs

The above discussion pertains to the deterministic analysis of one sphere pack, and it allows the rapid estimation of the influence of d_{50}, q, and r_c on $T_{applied}$. However, this analysis did not address the potential influence of ε, random variations in sphere packing and U_i on $T_{applied}$. These issues can only be quantified by conducting

pore-scale flow simulations on multiple realizations of a given sphere size distribution, and this produces uncertainty in the simulated value of the CDF of $T_{applied}$. In addition, scaling methods to predict the CDF of $T_{applied}$ for such conditions must relax the assumption of identical pore geometries, and results should therefore be viewed as only a first approximation to expected behavior.

It is logical to anticipate that ε will influence $T_{applied}$ because the average pore water velocity (v_{avg}) increases with decreasing ε. The influence of such variations in velocity on the CDF of $T_{applied}$ was previously demonstrated in Fig. 2c for a given sphere pack. We hypothesize that the influence of ε on v_{avg} can be simply accounted for by replacing q with $v_{avg} = q/\varepsilon$ in Eq. [23] as:

$$\left\langle T_{applied2} \right\rangle = \left\langle T_{applied1} \right\rangle \left(\frac{d_1}{d_2}\right)\left(\frac{q_2}{q_1}\right)\left(\frac{\varepsilon_1}{\varepsilon_2}\right) \quad [24]$$

This scaling approach assumes that ε will not influence the shape of the CDF of $T_{applied}$ due to random variations in the pore space geometry and sphere packing. To assess this potential limitation, simulations were run for five different realizations of two porosities (ε = 0.28 and 0.36) that employed the same values of $v_{avg} = 2.8 \times 10^{-5}$ m s^{-1} ($q = 8.8\times 10^{-6}$ and 1×10^{-5} m s^{-1} for ε = 0.28 and 0.36, respectively), $r_c = 0.5$ μm, $d_{50} = 100$ μm, and $U_i = 1$. The average value and confidence interval (±1 SD) of the CDF of $T_{applied}$ was determined and is shown in Fig. 4. The value of the CDF of $T_{applied}$ for the two porosities (ε = 0.28 and 0.36) was within the confidence interval (±1 SD) when the simulations were conducted using the same v_{avg}. This observation suggests that the packing porosity had a minor impact on the shape of the CDF for the considered conditions, and that Eq. [24] provides a reasonable first approximation to account for the influence of ε on the CDF of $T_{applied}$.

The influence of random variations in packing on the CDF of $T_{applied}$ was further assessed through repeated realizations (total of 5) of the sphere pack and simulation of the flow field shown in Fig. 1. The value of the CDF of $T_{applied}$ for each realization was quantified, and the mean value and confidence interval for the CDF of $T_{applied}$ for the ensemble realizations are shown in Fig. 5. The standard deviation ranged from 5.9×10^{-22} to 6.3×10^{-20} N m at the lowest and highest velocities, respectively, suggesting significant variability among the different realizations. It should also be noted that the confidence interval is much larger than that shown in Fig. 4 for the homogeneous sphere pack, suggesting that greater variability occurs with a larger grain size distribution (U_i = 2.08 compared with U_i = 1). Some of this packing variability is inherent to the software algorithm that was used to generate the sphere packs. A larger number of spheres (>25 spheres) is desirable to achieve a statistically representative pack for increasing values of U_i. Unfortunately, the current computational limitations at our desired simulation resolution made this undertaking unrealistic on our computer system.

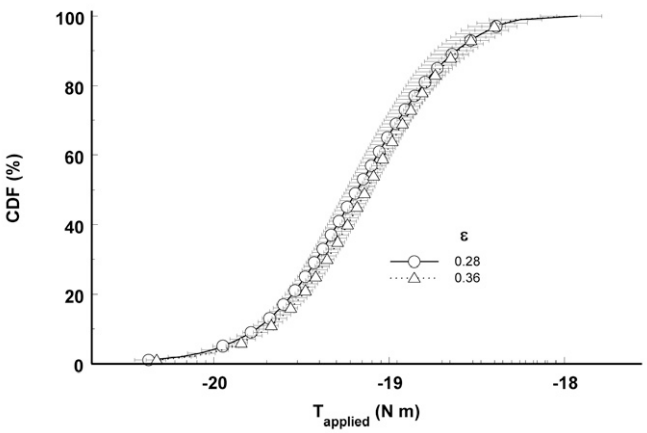

Fig. 4. The cumulative density function (CDF) for the applied hydrodynamic torque ($T_{applied}$) for when $r_c = 0.5$ μm, $d_{50} = 100$ μm, U_i = 1, $v_{avg} = 2.8 \times 10^{-5}$ m s^{-1}, and the porosity was varied (ε = 0.28 and 0.36). Simulations were run for five different realizations of a given porosity, and the average value of the CDF of $T_{applied}$ was determined and is shown, along with the confidence intervals (±1 SD). The x axis of the figure is plotted on a log scale, and the numbers shown are the power of the base 10 exponent.

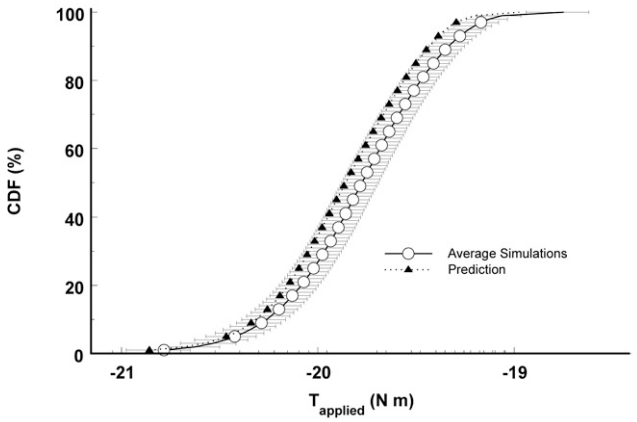

Fig. 5. The cumulative density function (CDF) for the applied hydrodynamic torque ($T_{applied}$) for the same simulation conditions as in Fig. 1c. In this case, the uncertainty in the CDF was quantified through repeated realizations and flow simulations (total of 5) of the sphere pack, and the mean value and confidence interval of ensemble realizations are shown. Also shown in the figure is the predicted CDF using Eq. [21] and [25] with $<T_{applied1}> = 1.12 \times 10^{-19}$ N m and σ = 0.99. The x axis of the figure is plotted on a log scale, and the numbers shown are the power of the base 10 exponent.

In an attempt to overcome this limitation, the CDF of $T_{applied}$ in porous media having a distribution of sphere sizes was predicted from corresponding information from uniform sphere packs using a modified form of Eq. [24] given as:

$$\left\langle T_{applied2} \right\rangle = \left\langle T_{applied1} \right\rangle \left(\frac{q_2}{q_1}\right)\left(\frac{\varepsilon_1}{\varepsilon_2}\right) d_1 \sum_{i=1}^{N} \frac{A_{fi}}{d_{2i}} \quad [25]$$

where A_{fi} is the fraction of the total solid surface area that is contributed by spheres of diameter d_{2i} that are associated with the ith class, and N is the total number of classes. This approach assumes that the contribution of a given sphere size class to $<T_{applied2}>$ is weighed by A_{fi} and that the value of σ is independent of U_i. The validity of these assumptions is assessed in Fig. 5 by comparison of the simulated value of $T_{applied}$ with the predicted value from Eq. [25]. The simulated and predicted value of $T_{applied}$ agreed reasonably well, with the prediction within the confidence interval of the simulated values and $R^2 = 0.96$.

A first approximation of the influence of variations in the grain size distribution on the predicted CDF of $T_{applied}$ was investigated using Eq. [25] assuming $r_c = 0.5$ μm, $d_{50} = 500$ μm, ε = 0.3, and $q = 8.4 \times 10^{-6}$ m s^{-1}, and the reference CDF of $T_{applied}$ shown in Fig. 4 ($<T_{applied1}> = 1.12 \times 10^{-19}$ N m and σ = 0.99). The distribution of sphere sizes consisted of uniform mass fractions ($1/N$) in each sphere class size, and N = 1, 11, 15, 17, and 19 when U_i = 1, 2.08, 3.14, 4.15, and 6, respectively. The values of A_{fi} and d_{2i} were calculated directly from the known size distribution of these sphere packs. Predicted results for the CDF of $T_{applied}$ are presented in Fig. 6. Equation [25] predicts that $<T_{applied2}>$ increases with U_i because smaller grain sizes (in a given volume) are associated with higher velocities near the SWI (Fig. 2b) and larger solid surface areas. It should be emphasized that the sphere size distributions were highly idealized in these simulations, and therefore care should be employed in attempts to extend this information to more complex grain size distributions of natural porous media.

Determining S_f and S_{max}

The value of S_f can easily be determined from Eq. [21–25] by simply setting $T_{applied}$ equal to a given value of $T_{adhesion}$ as:

$$S_f = \frac{1}{2} + \frac{1}{2}\text{erf}\left[\frac{\ln(T_{adhesion}) - \mu}{\sigma\sqrt{2}}\right] \quad [26]$$

Hence, information presented in Fig. 1 through 6 can also be used to determine S_f. As mentioned earlier, the value of $T_{adhesion}$ can be determined from DLVO calculations and Eq. [6–11]. Table 1 provides values of $T_{adhesion}$ for various values of r_c and ionic strength (IS) when using Eq. [11] in conjunction with published measurements (Shen et al., 2008) of the zeta potential of collector grains and colloids, and DLVO calculations to determine the depth of the secondary minimum. Notice that $T_{adhesion}$ increases with r_c and IS. Values of $T_{adhesion}$ ranged from 7.27×10^{-23} to 1.93×10^{-19} N m and clearly overlap with values of $T_{applied}$ shown in Fig. 1 through 6. This finding indicates that only a fraction of the solid surface may contribution to colloid retention (e.g., S_f), and that this fraction will depend on the grain size, colloid size, Darcy velocity, and IS due to their influence on $T_{applied}$ and $T_{adhesion}$. The above conclusions are expected to hold for alternative formulations of $T_{adhesion}$, such an empirical value of μ_f in Eq. [9] or the use of Eq. [10], although the exact magnitude of S_f for given system conditions will change.

Table 1. Values of $T_{adhesion}$ obtained for various r_c and ionic strength (IS) when using Eq. [6], [7], and [11] in conjunction with published measurements (Shen et al., 2008) of the zeta potential of the collector grains and colloids, and Derjaguin–Landau–Verwey–Overbeek (DLVO) calculations to determine the depth of the secondary minimum (Φ_{2min}).

r_c	IS	Φ_{2min}	h	$T_{adhesion}$
μm	mM	$k_B T_K$	nm	N m
0.015	100	0.51	5.15	7.27E-23
0.015	200	1.05	2.87	4.15E-22
0.578	10	1.54	26.03	1.24E-22
0.578	100	19.60	5.12	3.21E-20
0.578	200	41.30	2.81	1.93E-19

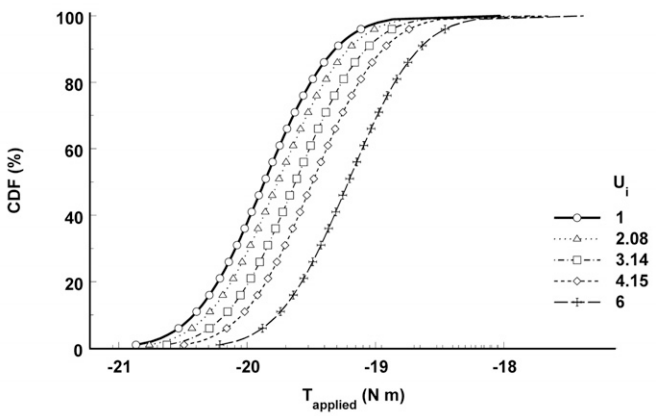

Fig. 6. The predicted cumulative density function (CDF) for the applied hydrodynamic torque ($T_{applied}$) for various grain size distributions (U_i = 1, 2.08, 3.14, 4.15, and 6) when $r_c = 0.5$ μm, $d_{50} = 500$ μm, ε = 0.3, and $q = 8.4 \times 10^{-6}$ m s^{-1}. The prediction was obtained using Eq. [21] and [25] with $<T_{applied1}> = 1.12 \times 10^{-19}$ N m and σ = 0.99. The values of A_{fi} and d_{2i} in Eq. [25] were calculated directly from the known size distribution of these sphere packs.

Figure 7 presents an example application of the torque balance approach to the pore-scale simulation results shown in Fig. 1 when $T_{adhesion}$ equals 3.2×10^{-20} and 1×10^{-19} N m. In this figure the red dots on the SWI indicate regions where colloid immobilization may occur because $T_{applied}$ is less than $T_{adhesion}$. Notice in Fig. 7a that these locations occur in low velocity regions near grain–grain contacts and small pore spaces when $T_{adhesion}$ equals 3.2×10^{-20} N m. These simulation results are consistent with experimental observation of colloid retention in micromodel studies under highly unfavorable attachment conditions (Bradford et al., 2005, 2006a; Xu et al., 2006; Li et al., 2006; Yoon et al., 2006; Gaillard et al., 2007; Tong et al., 2008). In contrast, nearly all of the SWI contributes to colloid retention in Fig. 7b when $T_{adhesion} = 1 \times 10^{-19}$ N m.

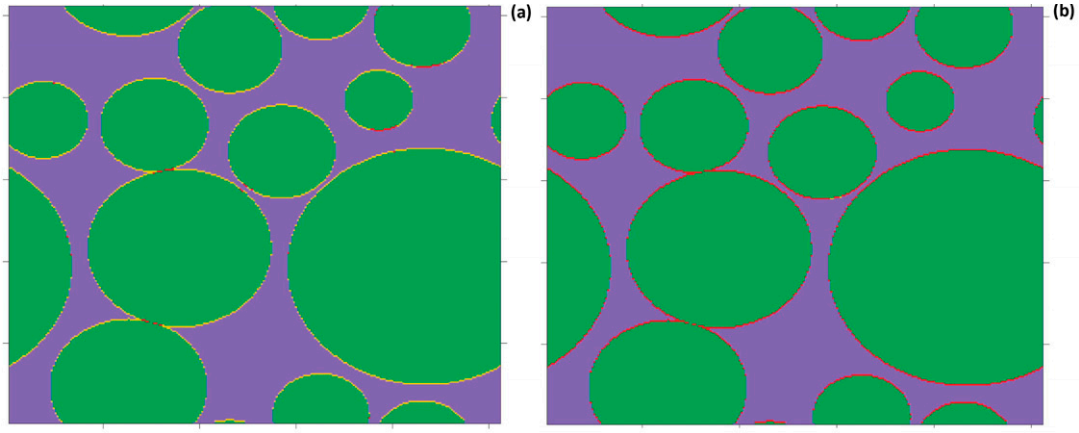

Fig. 7. An example application of the torque balance approach to the pore-scale simulation results shown in Fig. 1 when the adhesive torque ($T_{adhesion}$) equals 3.2×10^{-20} (Fig. 7a) and 1×10^{-19} N m (Fig. 7b). The red dots on the SWI indicates regions where colloid immobilization may occur because the applied hydrodynamic torque ($T_{applied}$) is less than $T_{adhesion}$.

The above S_f information may be used to directly determine S_{max} using the following relationship (Bradford et al., 2009; Kim et al., 2009):

$$S_{max} = \frac{(1-\gamma) A_s S_f}{A_c \rho_b} \quad [27]$$

where A_s [L^{-1}] is the geometric surface area per volume of porous medium, A_c [$L^2 N_c^{-1}$, and N_c denotes number of colloids] is the cross-section area per colloid, ρ_b [$M L^{-3}$] is the bulk density, and γ is the porosity of the colloid packing in a monolayer. The value of S_{max} is needed to predict the time and concentration dependence of the attachment coefficient using the Langmuirian blocking function (Adamczyk et al., 1994), and it has commonly been considered to be an empirical parameter that is typically determined by optimization to experimental results (Bradford et al., 2006b). Alternatively, the value of S_{max} can be converted to a pore volume fraction of retained colloids as $(\rho_b S_{max} V_c)/\varepsilon$, where V_c [$L^3 N_c^{-1}$] is the volume of the colloid.

Summary and Conclusions

Colloid retention in porous media depends on the forces and torques that act on colloids near the solid–water interface. The influence of the applied hydrodynamic torque on colloid retention can be significant under unfavorable attachment conditions, causing colloids to roll, skip, detach, or immobilize on the solid surface. Pore-scale simulations and theory presented here allowed us to predict the cumulative density function of the applied hydrodynamic torque for various colloid sizes, water flow rates, grain sizes, and grain size distributions. This information was then used in conjunction with the resisting adhesive torque to predict the fractions of the solid surface where colloids will be immobilized (e.g., S_f) and where they will be mobile (e.g., $1 - S_f$). The value of S_f is currently known to be needed to predict the time and concentration dependence of the attachment coefficient. Additional research is warranted to further utilize values of $(1 - S_f)$ and S_f in models of colloid transport and retention in saturated porous media. This is a topic of ongoing research.

Acknowledgments

This research was supported by the USDA (ARS, NP 206 and a grant from CSREES, NRI, 2006-02541).

References

Adamczyk, Z., B. Siwek, M. Zembala, and P. Belouschek. 1994. Kinetics of localized adsorption of colloid particles. Adv. Colloid Interface Sci. 48:151–280.

Bergendahl, J., and D. Grasso. 1998. Colloid generation during batch leaching tests: Mechanics of disaggregation. Coll. Surf. A Physicochem. Eng. Aspects 135:193–205.

Bergendahl, J., and D. Grasso. 1999. Prediction of colloid detachment in a model porous media: Thermodynamics. AIChE J. 45:475–484.

Bergendahl, J., and D. Grasso. 2000. Prediction of colloid detachment in a model porous media: Hydrodynamics. Chem. Eng. Sci. 55:1523–1532.

Bezrukov, A., D. Stoyan, and M. Dargiel. 2001. Spatial statistics for simulated packings of spheres. Image Anal. Stereol. 20:203–206.

Bradford, S.A., H.N. Kim, B.Z. Haznedaroglu, S. Torkzaban, and S.L. Walker. 2009. Coupled factors influencing concentration dependent colloid transport and retention in saturated porous media. Environ. Sci. Technol. 43:6996–7002.

Bradford, S.A., J. Simunek, M. Bettahar, Y.F. Tadassa, M.Th. van Genuchten, and S.R. Yates. 2005. Straining of colloids at textural interfaces. Water Resour. Res. 41:W10404, doi:10.1029/2004WR003675.

Bradford, S.A., J. Simunek, M. Bettahar, M.Th. van Genuchten, and S.R. Yates. 2006b. Significance of straining in colloid deposition: Evidence and implications. Water Resour. Res. 42:W12S15, doi:10.1029/2005WR004791.

Bradford, S.A., and S. Torkzaban. 2008. Colloid transport and retention in unsaturated porous media: A review of interface-, collector-, and pore-scale processes and models. Vadose Zone J. 7:667–681.

Bradford, S.A., S. Torkzaban, and S.L. Walker. 2007. Coupling of physical and chemical mechanisms of colloid straining in saturated porous media. Water Res. 41:3012–3024.

Derjaguin, B.V., and L.D. Landau. 1941. Theory of the stability of strongly charged lyophobic sols and of the adhesion of strongly charged particles in solutions of electrolytes. Acta Physicochim. USSR 14:733–762.

Duffadar, R.D., and J.M. Davis. 2007. Interaction of micrometer-scale particles with nanotextured surfaces in shear flow. J. Colloid Interface Sci. 308:20–29.

Duffadar, R.D., and J.M. Davis. 2008. Dynamic adhesion behavior of micrometer-scale particles flowing over patchy surfaces with nanoscale electrostatic heterogeneity. J. Colloid Interface Sci. 326:18–27.

Elimelech, M., J. Gregory, X. Jia, and R.A. Williams. 1995. Particle deposition and aggregation measurement, modeling and simulation. Butterworth-Heinemann, Woburn, MA.

Fraunhofer Institut fur Techno- und Wirtschaftsmathematik ITWM. 2003. GeoDict User's Guide Release 3, 2003–2008.

Gaillard, J.F., C. Chen, S.H. Stonedahl, B.L.T. Lau, D.T. Keane, and A.I. Packman. 2007. Imaging of colloidal deposits in granular porous media by X-ray difference micro-tomography. Geophys. Res. Lett. 34:L18404, doi:10.1029/2007GL030514.

Goldman, A.J., R.G. Cox, and H. Brenner. 1967. Slow viscous motion of a sphere parallel to a plane wall: I. motion through a quiescent fluid. Chem. Eng. Sci. 22:637–651.

Johnson, K.L., K. Kendall, and A.D. Roberts. 1971. Surface energy and the contact of elastic solids. Proc. R. Soc. Lond. A 11:301–313.

Johnson, W.P., X. Li, and S. Assemi. 2007a. Deposition and re-entrainment dynamics of microbes and non-biological colloids during non-perturbed transport in porous media in the presence of an energy barrier to deposition. Adv. Water Resour. 30:1432–1454.

Johnson, W.P., X. Li, and G. Yal. 2007b. Colloid retention in porous media: Mechanistic confirmation of wedging and retention in zones of flow stagnation. Environ. Sci. Technol. 41:1279–1287.

Israelachvili, J.N. 1992. Intermolecular and surface forces. 2nd ed. Academic Press, London.

Kim, H.N., S.A. Bradford, and S.L. Walker. 2009. *Escherichia coli* O157:H7 transport in saturated porous media: Role of solution chemistry and surface macromolecules. Environ. Sci. Technol. 43:4340–4347.

Kuznar, Z.A., and M. Elimelech. 2007. Direct microscopic observation of particle deposition in porous media: Role of the secondary energy minimum. Colloids Surf. A Physicochem. Eng. Asp. 294:156–162.

Li, X., C.-L. Lin, J.D. Miller, and W.P. Johnson. 2006. Pore-scale observation of microsphere deposition at grain-to-grain contacts over assemblage-scale porous media domains using x-ray microtomography. Environ. Sci. Technol. 40:3762–3768.

Lindeburg, M.R. 2001. Civil engineering reference manual for the PE exam. Professional Publ., Belmont, CA.

O'Neill, M.N. 1968. A sphere in contact with a plane wall in a slow linear shear flow. Chem. Eng. Sci. 23:1293–1298.

Shen, C., Y. Huang, B. Li, and Y. Jin. 2008. Effects of solution chemistry on straining of colloids in porous media under unfavorable conditions. Water Resour. Res. 44:W05419, doi:10.1029/2007WR006580.

Snyder, L.J., and W.E. Stewart. 1966. Velocity and pressure profiles for newtonian creeping flow in regular packed beds of shapes. AIChE J. 12:161–173.

Soltani, M., and G. Ahmadi. 1994. On particle adhesion and removal mechanics in turbulent flows. J. Adhes. Sci. Technol. 8:763–785.

Tafreshi, H.V., M.S. Rahman, S. Jaganathan, Q. Wang, and B. Pourdeyhimi. 2009. Analytical expressions for predicting permeability of bimodal fibrous porous media. Chem. Eng. Sci. 64:1154–1159.

Tong, M., H. Ma, and W.P. Johnson. 2008. Funneling of flow into grain-to-grain contacts drives colloid–colloid aggregation in the presence of an energy barrier. Environ. Sci. Technol. 42:2826–2832.

Toride, N., F.J. Leij, and M.Th. van Genuchten. 1995. The CXTFIT code for estimating transport parameters from laboratory and field tracer experiments. Res. Rep. 137. USDA-ARS, U.S. Salinity Lab., Riverside, CA.

Torkzaban, S., S.A. Bradford, and S.L. Walker. 2007. Resolving the coupled effects of hydrodynamics and DLVO forces on colloid attachment to porous media. Langmuir 23:9652–9660.

Torkzaban, S., H.N. Kim, J. Simunek, and S.A. Bradford. 2010. Hysteresis of colloid retention and release in saturated porous media during transients in solution chemistry. Environ. Sci. Technol. 44:1662–1669.

Torkzaban, S., S.S. Tazehkand, S.L. Walker, and S.A. Bradford. 2008. Transport and fate of bacteria in porous media: Coupled effects of chemical conditions and pore space geometry. Water Resour. Res. 44:W04403, doi:10.1029/2007WR006541.

Torkzaban, S., S.L. Walker, and S.A. Bradford. 2009. Reply to comment by William P. Johnson et al. on "Transport and fate of bacteria in porous media: Coupled effects of chemical conditions and pore space geometry". Water Resour. Res. 45:W09604, doi:10.1029/2008WR007576.

Torquato, S. 2002. Random heterogeneous materials: Microstructure and macroscopic properties. Springer, New York.

Tsai, C.J., D.Y.H. Pui, and B.Y.H. Liu. 1991. Particle detachment from disk surfaces of computer disk drives. J. Aerosol Sci. 22:737–746.

Vaidyanathan, R., and C. Tien. 1988. Hydrosol deposition in granular beds. Chem. Eng. Sci. 43:289–302.

Verwey, E.J.W., and J.Th.G. Overbeek. 1948. Theory of the stability of lyophobic colloids. Elsevier, Amsterdam.

Wiegmann, A. 2007. Computation of the permeability of porous materials from their microstructure by FFF-Stokes Available at http://www.forschungsplattform.de/zentral/download/berichte/bericht129.pdf (verified 7 Dec. 2010). Bericht des Fraunhofer ITWM 127. Fraunhofer-Institut für Techno- und Wirtschaftsmathematik ITWM, Kaiserslautern, Germany.

Wiegmann, A., and K.P. Bube. 2000. The explicit–jump immersed interface method: Finite difference methods for PDE with piecewise smooth solutions. SIAM J. Numer. Anal. 37:827–862.

Xu, S., B. Gao, and J.E. Saiers. 2006. Straining of colloidal particles in saturated porous media. Water Resour. Res. 42:W12S16, doi:10.1029/2006WR004948.

Yang, C., T. Dabros, D. Li, J. Czarnecki, and J.H. Masliyah. 1998. Kinetics of particle transport to a solid surface from an impinging jet under surface and external force fields. J. Colloid Interface Sci. 208:226–240.

Yoon, J.S., J.T. Germaine, and P.J. Culligan. 2006. Visualization of particle behavior with a porous medium: Mechanisms for particle filtration and retardation during downward transport. Water Resour. Res. 42:W06417, doi:10.1029/2004WR003660.